Hindawi
Mathematical Problems in Engineering
Volume 2019, Article ID 6362835, 12 pages
https://doi.org/10.1155/2019/6362835

Research Article

Research on Instability Boundaries of Control Force for Trajectory Correction Projectiles

Rupeng Li, Dongguang Li, and Jieru Fan

Science and Technology on Electromechanically Dynamic Control Laboratory, Beijing Institute of Technology, Beijing 100081, China

Correspondence should be addressed to Dongguang Li; lidongguang@bit.edu.cn

Received 29 August 2018; Revised 1 February 2019; Accepted 24 February 2019; Published 11 March 2019

Academic Editor: Kauko Leiviskä

The balance of stability and maneuverability is the foundation of the trajectory correction projectile. For the terminal correction projectile without an attitude feedback loop, a larger control force is expected which may cause an instability. This paper proposes a novel method to derive instability boundaries for the control force magnitude. No additional coordinate system is needed in this method. By introducing the concept of angular compensation matrix, the exterior ballistic linearized equations considering control force are established. The necessary prerequisite for a stable flight under control is given by the Routh stability criterion. The instability boundaries for the control force magnitude are derived. The results of example flights are 13.5% more accurate compared with that in relevant research. Numerical simulations demonstrate that if the control force magnitude lies in the unstable scope derived in this paper, the projectile loses its stability. Furthermore, the effects of the projectile pitch, velocity, and roll rate on flight stability during correction are investigated using the proposed instability boundaries.

1. Introduction

Trajectory correction projectiles/fuzes can meet the requirement of low collateral damage and higher delivery accuracy in modern warfare. Moreover, existing stockpiles can be retrofitted and upgraded by just replacing a trajectory correction fuze with a low cost [1–3]. So it is no doubt that trajectory correction technologies have received much attention from researchers. Numerous correction models such as impact point prediction [4–7] and model trajectory prediction [8–10] can be found in the literature. For the pursuit of further improvements in accuracy, the guidance law based on target imager feedback is proposed and becomes a tendency in the future [11, 12]. Unlike the scheme mentioned above, this correction strategy can be used only during the terminal phase with a limited time-to-go. Therefore, a larger control force is expected. However, that may cause an instability for the projectile under control. For a successful terminal correction, the balance between the maneuverability and stability for the projectile under control is studied in this paper.

Many efforts related to stability for ballistic flight have been explored in the literature. McCoy, R. L. [13], and Murphy [14–16] proposed the stability criteria for flight without control. Costello M [17] extended the gyro stability factor and dynamic stability factor to dual-spin projectile by linearization. In the area of flight stability with control, Wernert [18, 19] found that the control force induced by canards exerted an influence on steady angle of attack compared with conventional projectile without control. Cooper G and Fresconi F [20] regarded the projectile with activating canards asymmetric and investigated its flight stability under control. They established dynamic equations in the body reference frame. The research illustrated that flight instability would be caused when the control frequencies of actuator are close to fast epicyclic motion frequencies or slow epicyclic motion frequencies. Murphy [21] derived the stability boundaries for the maximum trim angles induced by control force. D Zhu [22] extended Murphy's work through Hurwitz stability criterion and derived an analytic solutions of stability boundaries.

The corresponding research made a significant contribution in the field of flight stability for controlled projectile. However, they did not reveal the relationship between control force magnitude and flight stability. Unlike missiles, the trajectory correction projectiles are not provided with a

feedback loop for flight attitude. The investigation of force magnitude influence on the stability is more urgent for such projectiles and is beneficial to the design of actuator (such as the canard deflection or reference area). Lloyd K.H [23] made some efforts in this aspect. By proposing the non-spinning coordinate originally, the research investigated the influence of force magnitude on the flight stability and derived the analytic damping rate expression of the projectile under control by an analogy to non-controlled projectile. However, such an analogy can only get a rough scope of the control force for flight stability.

This paper continues to bridge the gap in the area of controlled projectile stability and extend Lloyd K.H's research without utilizing the non-spinning coordinate. Exterior ballistic differential equations for controlled projectile are expressed in fixed-plane coordinate and rewritten as the form of coefficient matrix. The items of control force are retained in these equations by a novel angular compensation matrix. Routh stability criterion is applied to the coefficient matrix. The magnitude boundaries of the control force that result in flight instability are derived and analyzed.

In Section 2, dynamical equations for projectile under control are established by the proposed compensation matrix. In Section 3, the instability boundaries of the control force are presented on the basis of the Routh stability criterion. In Section 4, an example controlled flight is calculated and 6 DOF numerical simulations are implemented. The results are favorable. The influence of flight parameters on the stability is analyzed by the instability boundaries.

2. Projectile Flight Dynamic Model

This section introduces the concept of the trajectory correction projectile, establishes the equations of motion in fixed plane coordinate, and demonstrates the invalidity of the classical linearization in stability research. The cause is analyzed in deep and a novel linearized method based on compensation matrix that is proposed.

2.1. Concept of the Trajectory Correction Projectile. The trajectory correction projectile discussed in this paper is used to improve the operational capability of the artillery when attacking the ground targets. The correction actuator is integrated into the projectile fuze in our design. Its appearance is shown in Figure 1. The fuze consists of two parts defined as the forward part and aft part, respectively. The aft part is shown in green. It is fixedly connected with the projectile body by threaded connection. The projectile body is not illustrated here to highlight the fuze appearance. The forward part is shown in purple. It can rotate relative to the aft part of the fuze and the projectile body. The white nose represents the imager and is used for target detection. The blue part is the canard of a waffle style, in which each inner grid has a fixed deflection. It is strapdown with the forward fuze. When the projectile is in its ballistic flight, the canard is attached to the fuze surface. Once the correction is needed, the canard should be unfolded. Because of the oncoming flow and the deflection angle, the canard can produce an aerodynamic force which is used for projectile control. The direction of this control force is determined by roll angel of the forward fuze. Figure 2 illustrates the internal structure of the fuze. The red part represents a pair of bearings, which are used in providing a prerequisite for the relative rotation between the forward and aft part. The yellow part represents the motor shaft and gears, which are used to transfer the motor torque for the rotation.

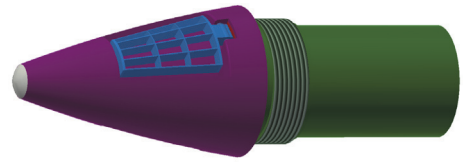

Figure 1: Appearance of the projectile fuze.

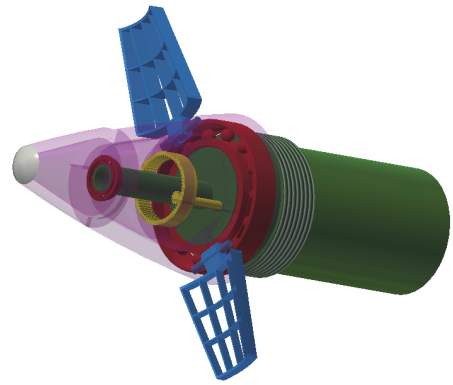

Figure 2: Internal structure of the projectile fuze.

When the projectile enters its descent trajectory, the detector starts to seek the target. The deviation between the target and the optical axis of detector is presented in detector imaging plane. The target orientation can be directly used to determine the roll angle of the forward fuze and as the input of the control system. The unfolding time of the canard depends on the magnitude of the deviation and the trajectory response under control. It can be seen that the correction actuator can complete the two-dimensional correction by a single motor.

In general, conventional projectiles for artillery can be equipped with the proposed fuze and subsequently obtain a correction capability. Such trajectory correction projectiles work during the terminal trajectory because of the limited detection distance. So the left flight time for correction is constrained. Therefore, a sufficient control force is more necessary here for an effective correction. That is why the canard has a waffle configuration for more frontal area. For stability that is no less important than maneuverability for such projectiles, the balance between them is investigated in this paper.

2.2. Flight Model of the Projectile. The projectile flight model is expressed by differential equations in fixed plane coordinate which is defined as follows: the origin of coordinate

system is located at the projectile centroid. X axis is aligned with the longitudinal axis of projectile, positive direction points to the projectile nose. Y axis is perpendicular to the longitudinal axis and lies in horizontal plane, positive direction points to right. Z axis is perpendicular to XY plane, positive direction points down. Projectile translational motion is written as follows:

$$\begin{Bmatrix} \dot{u} \\ \dot{v} \\ \dot{w} \end{Bmatrix} = \begin{Bmatrix} \frac{F_x}{m} \\ \frac{F_y}{m} \\ \frac{F_z}{m} \end{Bmatrix} + g \begin{Bmatrix} -\sin\theta \\ 0 \\ \cos\theta \end{Bmatrix} + \begin{Bmatrix} \frac{F_{xc}}{m} \\ \frac{F_{yc}}{m} \\ \frac{F_{zc}}{m} \end{Bmatrix} + \begin{Bmatrix} 0 & r & -q \\ -r & 0 & -r\tan\theta \\ q & r\tan\theta & 0 \end{Bmatrix} \begin{Bmatrix} u \\ v \\ w \end{Bmatrix} \tag{1}$$

Projectile angular motion is written as (2). F_{yc} and F_{zc} represent the horizontal and vertical components of the control force. M_C and N_C represent the corresponding control moments. While the canard is producing the control force, a drag force is also generated due to the canard deflection [18]. The induced drag force is denoted as F_{xc}. Generally, a small deflection angle is considered for trajectory correction projectiles with canard. In this situation, the induced drag force is far less than the induced control force. So it is always ignored. For the drag force induced by canard that is along the longitudinal axis and through projectile centroid, the corresponding moment is zero.

When the projectile is in a ballistic trajectory, the terms of control force and control moment are set to zero. And when the projectile needs a trajectory correction, these terms would have specific values according to operational requirements.

$$\begin{Bmatrix} \dot{p} \\ \dot{q} \\ \dot{r} \end{Bmatrix} = \left[I^{-1}\right] \left\{ \begin{Bmatrix} L \\ M \\ N \end{Bmatrix} + \begin{Bmatrix} 0 \\ M_c \\ N_c \end{Bmatrix} - \begin{bmatrix} 0 & -r & q \\ r & 0 & r\tan\theta \\ -q & -r\tan\theta & 0 \end{bmatrix} [I] \begin{Bmatrix} p \\ q \\ r \end{Bmatrix} \right\} \tag{2}$$

Angle of attack α and sideslip β are introduced and treated as small quantities. The expressions are shown as follows:

$$\alpha = \arctan^{-1}\left(\frac{w}{V}\right) \approx \frac{w}{V} \tag{3}$$

$$\beta = \arctan^{-1}\left(\frac{u}{V}\right) \approx \frac{u}{V} \tag{4}$$

Combining the latter two formulas in (1) and (2) with (3) and (4), a new equation set is completed. It is shown as follows:

$$\begin{aligned} \dot{\beta} &= \frac{F_y}{mv} + \frac{F_{yc}}{mv} - r - r\dot{\alpha}\tan\theta \\ \dot{\alpha} &= \frac{F_z}{mv} + \frac{F_{zc}}{mv} + \frac{g}{v}\cos\theta + q + r\dot{\beta}\tan\theta \\ \dot{q} &= \frac{M + M_c}{I_Y} - pr\frac{I_X}{I_Y} - r^2\tan\theta \\ \dot{r} &= \frac{N + N_c}{I_Y} + pq\frac{I_X}{I_Y} + qr\tan\theta \end{aligned} \tag{5}$$

The projectile body forces in (1) are composed of drag, lift, and Magnus force (always treated as small quantity and ignored). The projectile body moments in (2) are composed of static moment, pitch/yaw damping moment, and Magnus moment. The specific expressions for projectile body forces and moments are shown as follows:

$$\begin{aligned} F_y &= -\frac{1}{2}\rho SV^2 C_l\beta - \frac{1}{2}\rho SV^2 C_D\beta - \frac{1}{2}\rho SV^2 C_{yp\alpha}\frac{pl}{V}\alpha \\ F_z &= -\frac{1}{2}\rho SV^2 C_l\alpha - \frac{1}{2}\rho SV^2 C_D\alpha + \frac{1}{2}\rho SV^2 C_{yp\alpha}\frac{pl}{V}\alpha \\ M &= \frac{1}{2}\rho SlV^2 C_{M\alpha}\alpha + \frac{1}{2}\rho SlV^2 C_{Mp\alpha}\frac{pl}{V}\beta \\ &\quad + \frac{1}{2}\rho SlV^2 C_{Mq}\frac{l}{V}q \\ N &= -\frac{1}{2}\rho SlV^2 C_{M\alpha}\beta + \frac{1}{2}\rho SlV^2 C_{Mp\alpha}\frac{pl}{V}\alpha \\ &\quad + \frac{1}{2}\rho SlV^2 C_{Mq}\frac{l}{V}r \end{aligned} \tag{6}$$

By comparing with the total projectile velocity V and the projectile roll rate p, the magnitude of projectile yaw rate r and pitch tangent $\tan\theta$ are several orders inferior. The product of r and $\tan\theta$ is a smaller value in (5). Therefore, the neglect of $r\tan\theta$ is a reasonable simplification. In addition, the total velocity and the roll rate change slowly compared with other parameters and are regarded as constant here. With the simplifications above, the four equations of (5) are largely linearized and uncoupled. Such simplifications and linearized methods are frequently used and helpful in exterior ballistics research. More details can be found in [17, 24].

Based on the linearization, we rewrote (5) in the following form: $\dot{X} = KX + Q$, in wihch the specific expression is shown as (7). K is the coefficient matrix, which is used to depict the projectile state. Because of the linearization, (7) becomes a set of differential equations with constant coefficients. And each unit in matrix K is invariable, which makes sure that the coefficients of corresponding eigenvalue equation are

constant and provide a prerequisite for the future analysis of stability.

$$\begin{bmatrix} \dot{\beta} \\ \dot{\alpha} \\ \dot{q} \\ \dot{r} \end{bmatrix} = \begin{bmatrix} A & B & 0 & -1 \\ -B & A & 1 & 0 \\ D & C & E & -p\dfrac{I_X}{I_Y} \\ -C & D & p\dfrac{I_X}{I_Y} & E \end{bmatrix} \begin{bmatrix} \beta \\ \alpha \\ q \\ r \end{bmatrix} + \begin{bmatrix} \dfrac{F_{yc}}{mV} \\ mg\cos\theta + \dfrac{F_{zc}}{mV} \\ \dfrac{M_C}{I_Y} \\ \dfrac{N_C}{I_X} \end{bmatrix} \tag{7}$$

where

$$\begin{aligned} A &= -\frac{\rho SVC_{l\alpha}}{2m} - \frac{\rho SVC_D}{2m} \\ B &= -\frac{\rho SC_{yp\alpha}pl}{2m} \\ C &= \frac{\rho SlV^2C_{M\alpha}}{2I_Y} \\ D &= \frac{\rho Sl^2VC_{MP\alpha}p}{2I_Y} \\ E &= \frac{\rho Sl^2VC_{Mq}}{2I_Y} \end{aligned} \tag{8}$$

It is remarkable that terms related to control force in (7) consist in matrix Q and its mathematical implications mean that the control force will cause a steady-state trim angle. This is in line with Wernert's research [18]. However, these terms would not appear in the coefficient matrix K. The phenomenon is caused by the linearization according to the definition of the fixed plane coordinate. The fixed plane coordinate should have a roll rate-$r\tan\theta$ relative to the inertial coordinate and it is the prerequisite to ensure that the y axis is located in the horizontal plane all the time. For ballistic trajectory without control force, the neglect of $r\tan\theta$ is a good assumption for linearization. But when control force is considered, the situation is different. Because once the target orientation relative to the projectile is determined, the control force direction would not vary. However, ignoring the item $-r\tan\theta$ forces the fixed plane coordinate rotate around its longitudinal axis at the roll rate $r\tan\theta$. This implies the direction of the control force and is changing along with the fixed plane coordinate constantly. So a contradiction is caused. When it is reflected by the coefficient matrix, there would be no difference in K between the ballistic and controlled trajectory, and the control force would not appear in matrix K. Therefore, for further study of controlled trajectory, the effect of the neglect of $-r\tan\theta$ should be compensated before linearization.

2.3. Compensation Matrix for Control Force. Based on the analysis in Section 2.1, the paper introduces an angular compensation matrix for control force and gravity to solve the problem above. We define the control force roll angle induced by linearization as Φ and express it as (9). The expression for roll angle induced by gravity has the same expression as follows:

$$\dot{\Phi} = r\tan\theta \tag{9}$$

The compensation matrix for control force and gravity is written as follows:

$$T_m = \begin{bmatrix} 1 & 0 & 0 \\ 0 & \cos\Phi & \sin\Phi \\ 0 & -\sin\Phi & \cos\Phi \end{bmatrix} \tag{10}$$

With the compensation matrix, the projectile translational motion is rewritten as follows:

$$\begin{Bmatrix} \dot{u} \\ \dot{v} \\ \dot{w} \end{Bmatrix} = \begin{Bmatrix} \dfrac{F_x}{m} \\ \dfrac{F_y}{m} \\ \dfrac{F_z}{m} \end{Bmatrix} + g \begin{bmatrix} 1 & 0 & 0 \\ 0 & \cos\Phi & \sin\Phi \\ 0 & -\sin\Phi & \cos\Phi \end{bmatrix} \begin{bmatrix} -\sin\theta \\ 0 \\ \cos\theta \end{bmatrix} + \begin{bmatrix} 1 & 0 & 0 \\ 0 & \cos\Phi & \sin\Phi \\ 0 & -\sin\Phi & \cos\Phi \end{bmatrix} \begin{bmatrix} \dfrac{F_{xc}}{m} \\ \dfrac{F_{yc}}{m} \\ \dfrac{F_{zc}}{m} \end{bmatrix} + \begin{Bmatrix} 0 & r & -q \\ -r & 0 & -r\tan\theta \\ q & r\tan\theta & 0 \end{Bmatrix} \begin{Bmatrix} u \\ v \\ w \end{Bmatrix} \tag{11}$$

The projectile angular motion is rewritten as follows:

$$\begin{Bmatrix} \dot{p} \\ \dot{q} \\ \dot{r} \end{Bmatrix} = \left[I^{-1}\right] \left\{ \begin{Bmatrix} L \\ M \\ N \end{Bmatrix} + \begin{bmatrix} 1 & 0 & 0 \\ 0 & \cos\Phi & \sin\Phi \\ 0 & -\sin\Phi & \cos\Phi \end{bmatrix} \begin{bmatrix} L_c \\ M_c \\ N_c \end{bmatrix} - \begin{bmatrix} 0 & -r & q \\ r & 0 & r\tan\theta \\ -q & -r\tan\theta & 0 \end{bmatrix} [I] \begin{Bmatrix} p \\ q \\ r \end{Bmatrix} \right\} \tag{12}$$

Then the latter two formulas in (11) and (12) can be linearized with the control force retained after the compensation. The projectile velocity V and roll rate p are regarded as constant in a sufficiently short time interval regarding the velocity component u equal to V. The pitch angle θ is substituted by $\theta_0+\theta_d$. θ_0 is the initial pitch angle. θ_d is a small departure from θ_0. It should be noted that this method is

applicable within a few seconds of the selected feature point. Fortunately, the time-to-go for terminal correction is limited to several seconds. The linear ballistic differential equations are eventually expressed as (13)-(16).

$$\dot{\beta} = \frac{F_y}{mV} + \left(\frac{F_{zc}}{mV} + \frac{g}{V}\cos\theta_0\right)\Phi - r + \frac{F_{yc}}{mV} \tag{13}$$

$$\dot{\alpha} = \frac{F_z}{mV} + \frac{F_{zc}}{mV} + \frac{g}{V}\cos\theta_0 + q - \frac{F_{yc}}{mV}\Phi - \left(\frac{g}{V}\sin\theta_0\right)\theta_d \tag{14}$$

$$\dot{q} = \frac{M}{I_Y} - pr\frac{I_X}{I_Y} + \frac{M_c}{I_Y} + \frac{N_c}{I_Y}\Phi \tag{15}$$

$$\dot{r} = \frac{N}{I_Y} + pq\frac{I_X}{I_Y} + \frac{N_c}{I_Y} - \frac{M_c}{I_Y}\Phi \tag{16}$$

Combining the four equations above with (9) and supplemental equation (17), the set of equations are completed.

$$\dot{\theta}_d = q \tag{17}$$

3. The Instability Boundary for Control Force

The purpose of this section is to derive the boundary for control force that causes an instability and makes some efforts to build the balance between the maneuverability and stability for the projectile under control.

We rewrite the set of equations (13)-(17) as matrix form: $\dot{X} = KX + Q$:

$$\begin{bmatrix} \dot{\beta} \\ \dot{\alpha} \\ \dot{q} \\ \dot{r} \\ \dot{\Phi} \\ \dot{\theta}_d \end{bmatrix} = \begin{bmatrix} A & B & 0 & -1 & F & 0 \\ B & A & 1 & 0 & G & H \\ D & C & E & -p\frac{I_X}{I_Y} & R & 0 \\ -C & D & p\frac{I_X}{I_Y} & E & S & 0 \\ 0 & 0 & 0 & \tan\theta_0 & 0 & 0 \\ 0 & 0 & 1 & 0 & 0 & 0 \end{bmatrix} \begin{bmatrix} \beta \\ \alpha \\ q \\ r \\ \Phi \\ \theta_d \end{bmatrix} + \begin{bmatrix} \frac{F_{yc}}{mV} \\ \frac{F_{zc}}{mV} + \frac{g}{V}\cos\theta_0 \\ \frac{M_C}{I_Y} \\ \frac{N_C}{I_X} \\ 0 \\ 0 \end{bmatrix} \tag{18}$$

where the new notations are as follows:

$$\begin{aligned} F &= \frac{F_{ZC}}{mV} + \frac{g}{V}\cos\theta_0 \\ G &= -\frac{F_{YC}}{mV} \\ H &= -\frac{g}{V}\sin\theta_0 \\ R &= \frac{N_C}{I_Y} \\ S &= -\frac{M_C}{I_Y} \\ T &= p\frac{I_X}{I_Y} \end{aligned} \tag{19}$$

Terms related to control force are now involved in the coefficient matrix K with the compensation matrix. The eigenvalue equation for the coefficient matrix in (18) is established as follows:

$$\det(\lambda \mathrm{E} - \mathrm{A}) = a_6\lambda^6 + a_5\lambda^5 + a_4\lambda^4 + a_3\lambda^3 + a_2\lambda^2 + a_1\lambda + a_0 \tag{20}$$

where a_0-a_6 are consisted of the terms A, B, C, etc. These terms are the combination of physical parameters, state parameters, and aerodynamic coefficients of the projectile. The physical parameters represent the inherent properties of a projectile. So they are constant. State parameters and aerodynamic coefficients could be regarded as constant as well in a short time interval. When a long-duration flight is considered, they should be updated periodically. Each constituent is complex and brings difficulties to calculation and analysis. However, the dominant terms are limited relatively. For simplicity, secondary factors are ignored. The feasibility of this simplification will be verified later. The expressions for a_0-a_6 after simplification are written here directly.

$$\begin{aligned} a_6 &= 1 \\ a_5 &= -2A - 2E \\ a_4 &= T^2 - 2C - S\tan\theta_0 \\ a_3 &= -2AT^2 + 2AC + 2CE + 2DT - RT\tan\theta_0 \\ a_2 &= C^2 + CS\tan\theta_0 - DR\tan\theta_0 + 2ART\tan\theta_0 \\ a_1 &= C^2H - C^2F\tan\theta_0 - ACS\tan\theta_0 + CHS\tan\theta_0 \\ a_0 &= -ACHS\tan\theta_0 - C^2FH\tan\theta_0 \end{aligned} \tag{21}$$

Table 1: Initial states and meteorological conditions.

Initial states		Meteorological conditions	
Velocity	250m/s	Ground pressure	1000hPa
Elevation	-43°	Virtual temperature	288.9
Direction	0°	Longitudinal wind	0m/s
Spin-rate	1050rad/s	Lateral wind	0m/s

The Routh matrix corresponding to the eigenvalue equation (20) is established.

$$T_{ROUTH} = \begin{bmatrix} a_6 & a_4 & a_2 & a_0 \\ a_5 & a_3 & a_1 & \\ b_1 = \frac{-1}{a_5}(a_6a_3 - a_5a_4) & b_2 = \frac{-1}{a_5}(a_6a_1 - a_2a_5) & b_3 = a_0 & \\ c_1 = \frac{-1}{b_1}(a_5b_2 - a_3b_1) & c_2 = \frac{-1}{b_1}(a_5b_3 - a_1b_1) & & \\ d_1 = \frac{-1}{c_1}(b_1c_2 - b_2c_1) & d_2 = a_0 & & \\ e_1 = \frac{-1}{d_1}(c_1d_2 - c_2d_1) & & & \\ f_1 = a_0 & & & \end{bmatrix} \quad (22)$$

The necessary prerequisite for a stable flight under control is given according to the Routh stability criterion: The coefficients a_0-a_6 in (20) are positive and the first column elements of the Routh matrix are positive. Furthermore, if the control force magnitude cannot meet (23), the projectile will lose its stability. Then the control force is defined as an unstable force. The set of all unstable forces is called unstable scope. The boundaries of the scope are denoted as the instability boundary. A conclusion is derived evidently that if a control force magnitude belongs to the unstable scope, the flight is definitely unstable.

$$\begin{gathered} a_5 > 0, \\ a_4 > 0, \\ a_3 > 0, \\ a_2 > 0, \\ a_1 > 0, \\ a_0 > 0 \\ b_1 > 0, \\ c_1 > 0, \\ d_1 > 0, \\ e_1 > 0 \end{gathered} \quad (23)$$

4. Verification and Results

This section demonstrates the feasibility and liability of the theory derived in Section 3. Generally, the flight instability can be clearly shown by numerical simulation. According to the research of Lloyd C.H [23], projectiles under control are the most sensitive to horizontal forces. Therefore, the simulations in this section pay emphasis on the effect of horizontal control force F_{yc}.

Table 2: Aerodynamic coefficients of the example projectile.

Aerodynamic coefficients	
lift force coefficient	1.7
drag force coefficient	0.13
Magnus force coefficient derivative	-1.5
static moment coefficient derivative	3.8
Magnus moment coefficient derivative	0.2
damping moment coefficient derivative	-8.0

The example projectile mass m is 15kg, moment of inertia for longitudinal axis I_x is 0.023kg·m^2, moment of inertia for projectile transverse axis I_y is 0.22kg·m^2, the reference area S is 0.0087m^2, and the projectile diameter d is 0.105m. Initial states and meteorological conditions are shown in Table 1. The aerodynamic coefficients of the example projectile are shown in Table 2

We take the example projectile to calculate the instability boundaries for the flight under control. The result of this unstable scope is $[-\infty, -35.48] \cup [58.33, +\infty]$. According to the theory in Section 3, when control force magnitude belongs to the unstable scope ($F_{yc} \in [-\infty, -35.48] \cup [58.33, +\infty]$), the projectile will lose its stability.

Before the verification by simulation, the simplification in Section 3 is recalled. It has been mentioned above that the result is derived from simplified a_0-a_6. To demonstrate the practicability of this simplification, the instability boundaries are calculated again without any simplification. The result is $F_{yc} \in [-\infty, -35.63] \cup [58.00, +\infty]$. It can be seen that the result varies a little compared with that of simplified model.

The projectile angular motion without control force is presented as Figure 3. The angle of attack motion and sideslip motion along with time are presented in Figure 4.

These two figures illustrate that the angular motions for the flight without control force are converging gradually along with time and represent a stable flight.

The projectile angular motion with a -55N force to left is presented as Figure 5. In the same case, the angle of attack motion and sideslip motion along with time are presented in Figure 6.

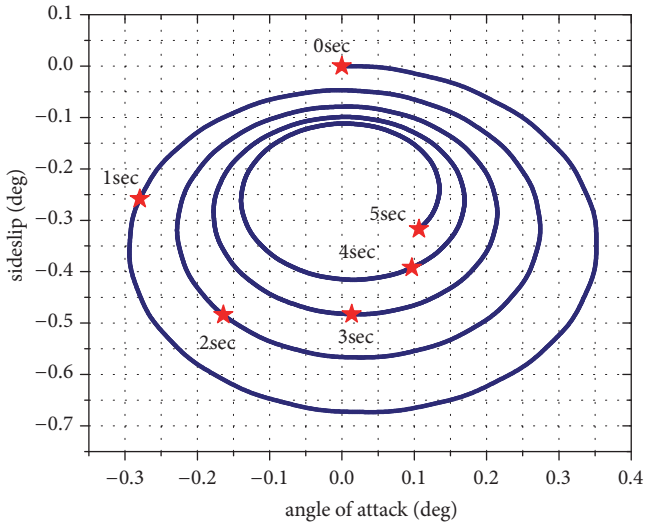

Figure 3: Angular motion for the flight without control force.

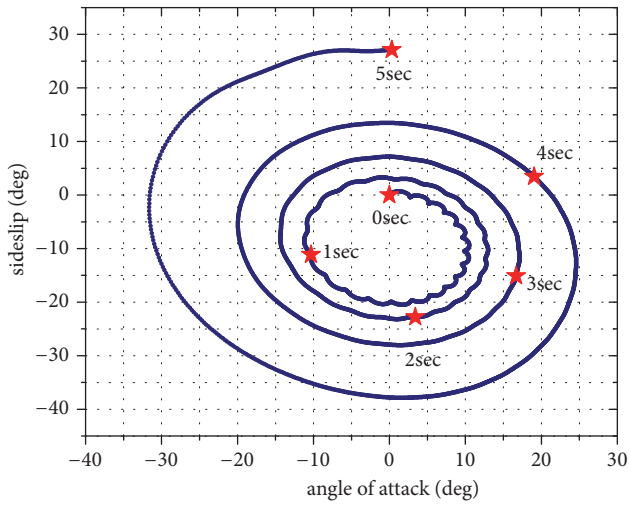

Figure 5: Angular motion for the flight with -55N control force.

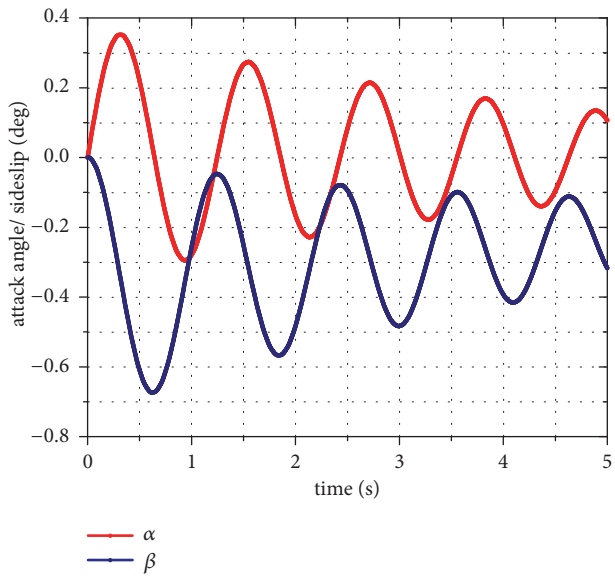

Figure 4: Angle of attack and sideslip for the flight without control force.

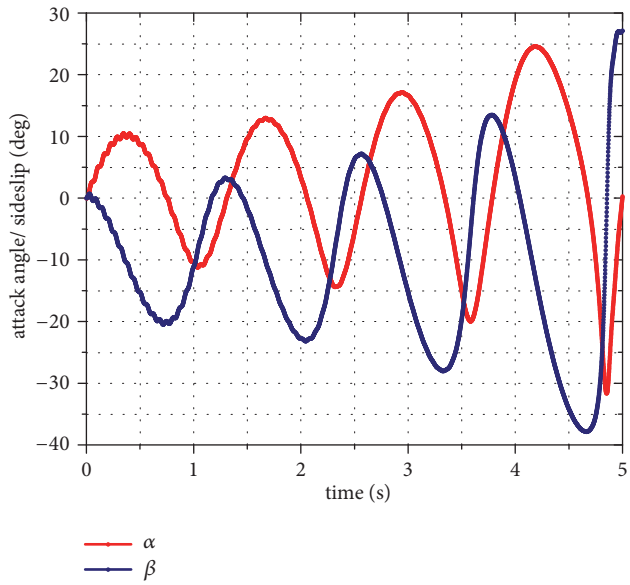

Figure 6: Angle of attack and sideslip for the flight with -55N control force.

In Figures 5 and 6, the fast epicyclic motion of the projectile is stable. However, the slow epicyclic motion is diverging along with time obviously. The results have illustrated that the slow epicyclic motion of the projectile is unstable when a -55N control force is exerted to left. The simulation results for $F_{yc} = -55 \in [-\infty, -35.63] \cup [58.00, +\infty]$ are in conformity to the negative part of the analytic instability boundaries.

Figures 7 and 8 present the numerical simulation results for the flight under an 80N control force. They illustrate that the slow epicyclic motion of the projectile is stable. However, the angle of attack and sideslip are diverging along with time obviously, and the fast epicyclic motion is unstable. For the control force 80N belonging to the unstable scope, the simulation results demonstrate the validity of the positive part of instability boundaries.

Additionally, the instability boundaries for the flight under control derived in this paper are compared with Lloyd's research. With the same example projectile, initial and meteorological conditions and the instability boundaries under horizontal control force by Lloyd are written as $F_{yc} \in [-\infty, -44.61] \cup [66.91, +\infty]$. As is shown in Figure 9, the blue slash represents the scope of horizontal control force that causes an instability derived by Lloyd, and the red slash represents the same scope derived in this paper.

The figure indicates that the instability boundaries in this paper extend the scope by 13.5% compared with Lloyd's research. To further demonstrate the reliability of this

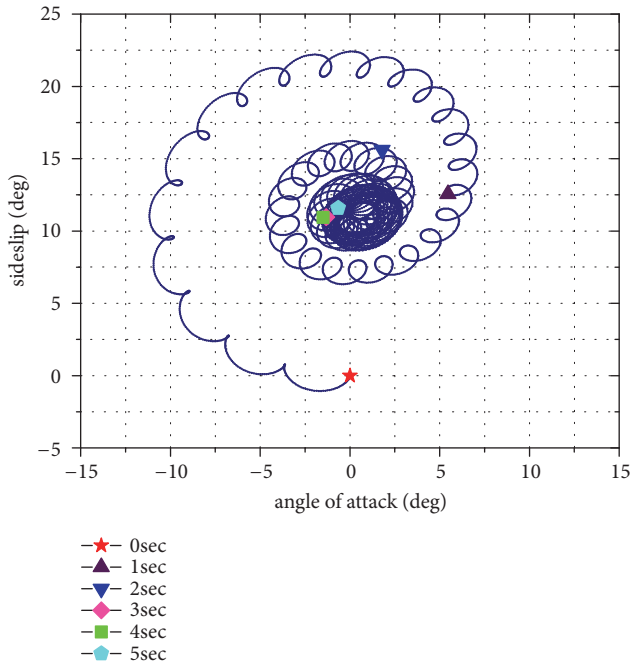

Figure 7: Angular motion for the flight with 80N control force.

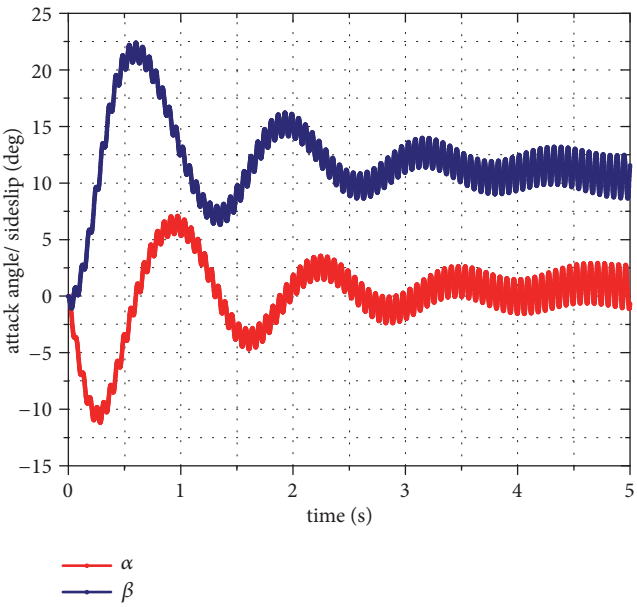

Figure 8: Angle of attack and sideslip for the flight with 80N control force.

method, another two simulations are implemented. The control force magnitude is chosen from the extended scope by comparison.

Figures 10 and 11 exhibit the angular motion, angle of attack, and sideslip for the flight with a -40N control force (the value -40 is in the negative extended scope by comparison). The numerical simulation result illustrates clearly that the flight is unstable (specifically, the fast epicyclic motion is stable, while the slow epicyclic motion is unstable).

Similarly, Figures 12 and 13 exhibit the angular motion, angle of attack, and sideslip for the flight with a 60N control force (the value 60 is in the positive extended scope by comparison). The numerical simulation result indicates that the flight is unstable (specifically, the slow epicyclic motion is stable, while the fast epicyclic motion is unstable).

The two simulation results give a further demonstration for the instability boundaries of the flight under control derived in this paper. In addition, it is 13.5% more accurate than Lloyd's research.

5. The Effect of Projectile Parameters on Instability Boundaries

The effects of the projectile parameters during flight on stability are analyzed and discussed, respectively, utilizing the instability boundaries when a control force is exerted.

5.1. The Initial Pitch θ_0. Figure 14 dictates the effect of initial pitch on the instability boundaries. The line of red triangle represents the lower instability boundary variation of the positive control force (denoted as lower boundary for short). The line of blue diamond represents the upper instability boundary variation of the negative control force (denoted as upper boundary for short). As presented in Figure 14, the lower boundary increases progressively as the initial pitch angle decreases in descending flight, while the upper boundary decreases.

The instability boundary variation in this case dictates a decreasing control force unstable scope. That is to say, the increase of the pitch angle in descending flight improves the projectile stability. The reason is that the pitch angle represents the curvature of the trajectory which will induce an aerodynamic trim angle. During the descending flight, the small pitch angle implies a severe trajectory curvature and a large trim angle. Therefore, the flight stability is weakened with the extra aerodynamic drag and lift forces induced by large trim angle.

5.2. The Projectile Velocity V. Figure 15 dictates the effect of projectile velocity on the instability boundaries. The lines of red triangle and blue diamond represent the lower boundary and upper boundary variation, respectively, along with projectile velocity. As illustrated in Figure 15, the increase of projectile velocity causes an increase in lower boundary and a decrease in upper boundary. As discussed in Figure 14, the result illustrates that the flight stability increases as the projectile velocity increases. The conclusion of the analysis is in line with the literature [25].

5.3. The Projectile Roll Rate p. The effect of projectile roll rate on the instability boundaries is illustrated in Figure 16. The expression is almost identical to Figure 15 and to avoid repetition; it is not described here. The increase of projectile velocity causes a lower boundary increase and an upper boundary decrease. That is to say, the flight stability is positively associated with the projectile roll rate. The result

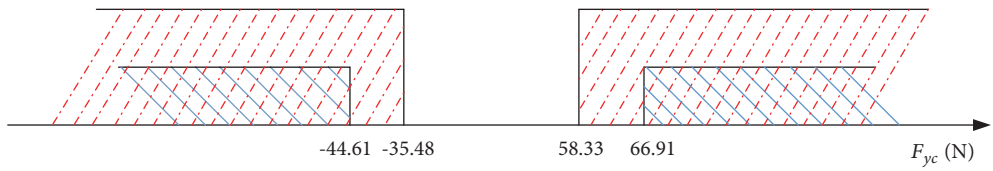

Figure 9: The comparison of instability boundaries.

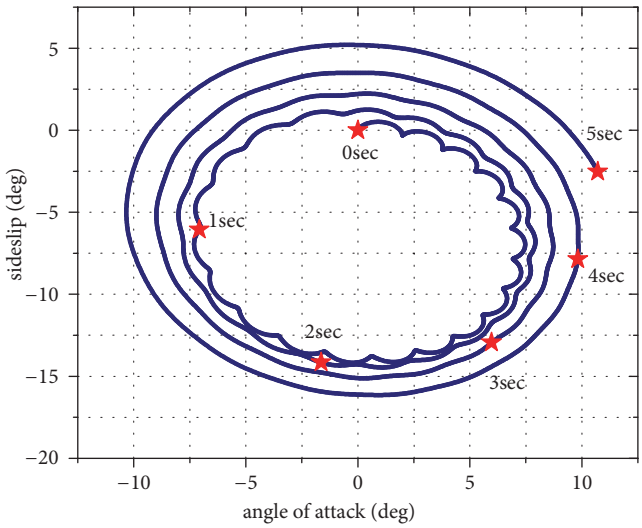

Figure 10: Angular motion for the flight with -40N control force.

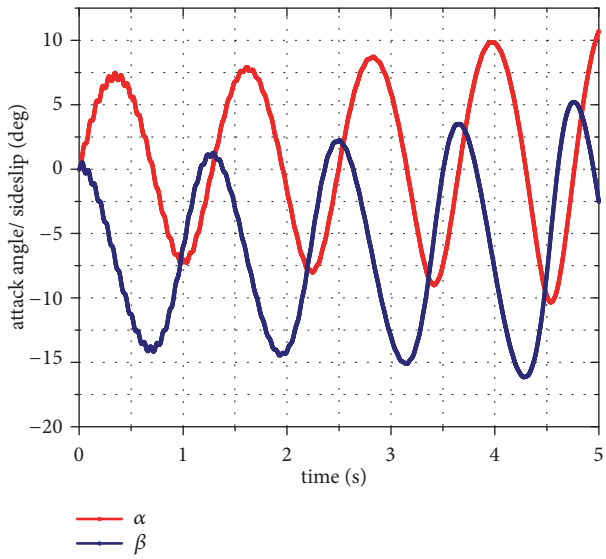

Figure 11: Angle of attack and sideslip for the flight with -40N control force.

is in line with the classical ballistic theory: the increase of projectile roll rate will directly improve the gyroscopic stability factor of projectiles.

This section shows the effects of projectile parameters on instability boundaries. The results illustrate that the proposed

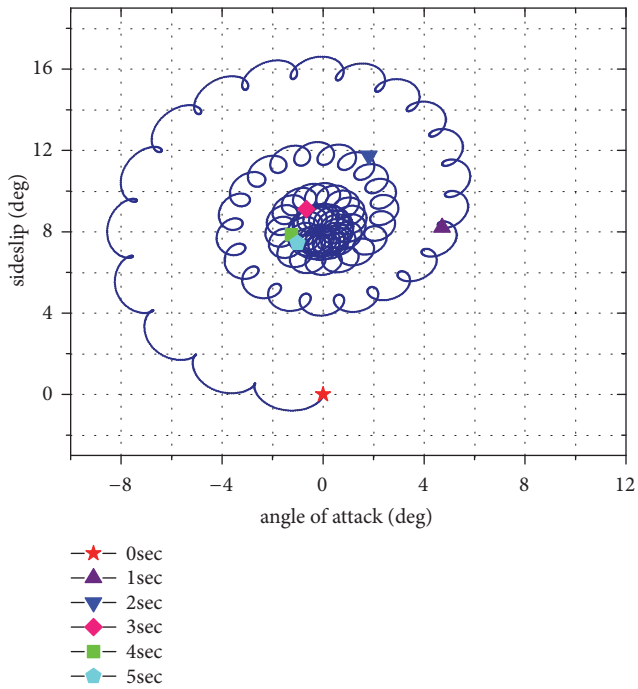

Figure 12: Angular motion for the flight with 60N control force.

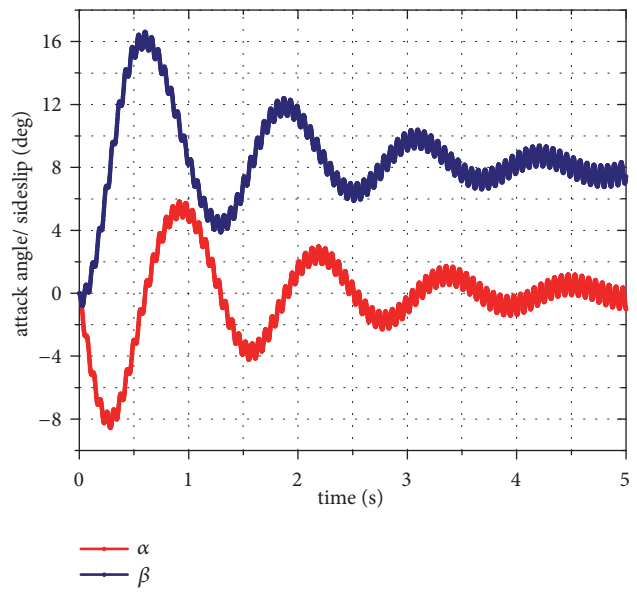

Figure 13: Angle of attack and sideslip for the flight with 60N control force.

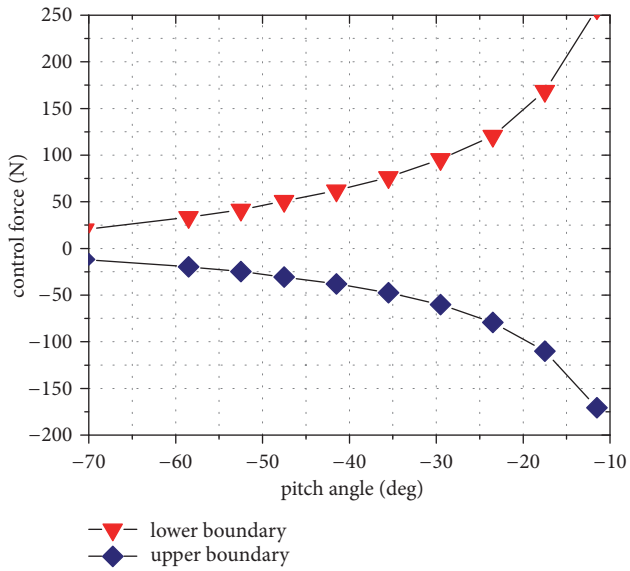

Figure 14: The effect of initial pitch angle on the instability boundaries.

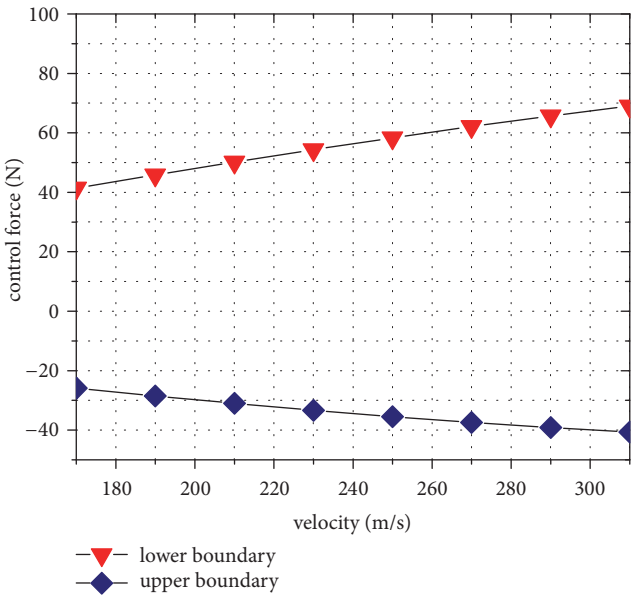

Figure 15: The effect of projectile velocity on the instability boundaries.

instability boundaries can be used to predict the stability variation under various flight parameters. The prediction results are in line with the relevant research or theory. Therefore, the validity of instability boundaries is demonstrated once again in this respect.

6. Conclusion

This work mainly focuses on the balance between the maneuverability and stability for the projectile under control. With a deep investigation, this paper indicates the invalidity of classical linearization in stability analysis and reveals the reason. Based on that, the exterior ballistic equations are established with the unique proposed compensation matrix and no additional coordinate system is needed. The necessary prerequisite for a stable flight under control is given by Routh stability criterion and the instability boundaries for the control force are derived. Numerical simulations demonstrate the validity of the analytic relationship between the flight instability boundaries and the control force magnitude. Additionally, the instability boundaries derived in this paper are compared with Lloyd's research. The comparison results dictate that the former is more accurate and extends the scope by 13.5%. The results are also verified by simulations. The effects of the projectile pitch, velocity, and roll rate on the instability boundaries are analyzed, respectively, when a control force is exerted. The results illustrate that the unstable scope is negatively associated with the all the three projectile parameters during the descending flight, while the projectile stability is positively associated.

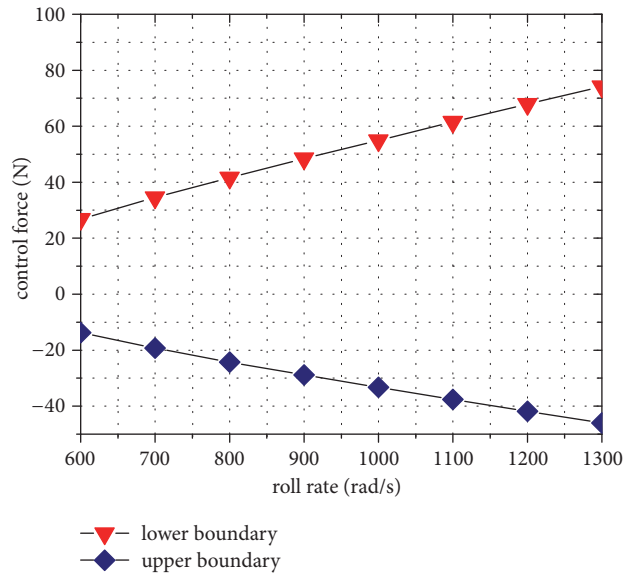

Figure 16: The effect of projectile velocity on the instability boundaries.

Nomenclature

C_l: Lift force coefficient
C_D: Drag force coefficient
$C_{yp\alpha}$: Magnus force coefficient derivative
$C_{M\alpha}$: Static moment coefficient derivative
$C_{Mp\alpha}$: Magnus moment coefficient derivative
C_{Mq}: Damping moment coefficient derivative induced by pitch and yaw rate
u, v, w: Projectile velocity component of x, y, z axis in fixed plane coordinate, m/s
F_x, F_y, F_z: Aerodynamic forces component on projectile body of x, y, z axis in fixed plane coordinate, N

F_{yc}, F_{zc}: Control forces component on projectile body of y, z axis in fixed plane coordinate, N
p, q, r: Projectile roll rate, pitch rate, yaw rate in fixed plane coordinate, rad/s
L, M, N: Aerodynamic moments component on projectile body of x, y, z axis in fixed plane coordinate, Nm
M_c, N_c: Control moments component on projectile body of y, z axis in fixed plane coordinate, Nm
V: Projectile velocity, m/s
θ: Projectile pitch angle, rad
g: Gravitational acceleration, m/s^2
ρ: Atmospheric density, kg/m^3
S: Projectile reference area, m^2
I_X: Moment of inertia for projectile longitudinal axis, kg·m^2
I_Y: Moment of inertia for projectile transverse axis, kg·m^2
$[I]$: Diagonal inertia matrix
l: Projectile reference length, m.

Data Availability

The data used to support the findings of this study are available from the corresponding author upon request.

Disclosure

This research received no specific grant from any funding agency in the public, commercial, or not-for-profit sectors.

Conflicts of Interest

The authors declare that there are no conflicts of interest regarding the publication of this article.

References

[1] E. Gagnon and M. Lauzon, "Course correction fuze concept analysis for in-service 155 mm spin-stabilized gunnery projectiles," in *Proceedings of the AIAA paper 2008-6997, Guidance, Navigation and Control Conference*, 2008.

[2] P. H. Morrison and D. S.Amberntson, "Guidance and control of a cannon-launched guided projectile," *Journal of Spacecraft and Rockets*, vol. 14, no. 6, pp. 328–334, 1977.

[3] C. Montalvo and M. Costello, "Effect of canard stall on projectile roll and pitch damping," in *Proceedings of the Institute of Mechanical Engineers, Part G: Journal of Aerospace Engineering*, vol. 225, pp. 703–716, 2011.

[4] F. Fresconi, "Guidance and control of a projectile with reduced sensor and actuator requirements," *Journal of Guidance, Control, and Dynamics*, vol. 34, no. 6, pp. 1757–1766, 2011.

[5] F. Fresconi and P. Plostins, "Control mechanism strategies for spin-stabilized projectiles," in *Proceedings of the Institution of Mechanical Engineers, Part G: Journal of Aerospace Engineering*, vol. 224, pp. 979–991, 2010.

[6] K. Pamadi and E. Ohlmeyer, "Evaluation of two guidance laws for controlling the impact flight path angle of a naval gun launched spinning projectile," in *Proceedings of the AIAA Paper 2006-6081, Guidance, Navigation and Control Conference*, 2006.

[7] C. A. Phillips, "Guidance algorithm for range maximization and time-of-flight control of a guided projectile," *Journal of Guidance, Control, and Dynamics*, vol. 31, no. 5, pp. 1447–1455, 2008.

[8] D. Ollerenshaw and M. Costello, "Model predictive control of a direct fire projectile equipped with canards," *Journal of Guidance, Control, and Dynamics*, vol. 130, no. 6, pp. 758–767, 2008.

[9] T. Jitpraphai and M. Costello, "Dispersion reduction of a direct fire rocket using lateral pulse jets," *Journal of Spacecraft and Rockets*, vol. 38, no. 6, pp. 929—936, 2001.

[10] J. Rogers and M. Costello, "Design of a roll-stabilized mortar projectile with reciprocating canards," *Journal of Guidance, Control, and Dynamics*, vol. 33, no. 4, pp. 1026–1034, 2010.

[11] F. Fresconi and J. Rogers, "Flight control of a small-diameter spin-stabilized projectile using imager feedback," *Journal of Guidance, Control, and Dynamics*, vol. 38, no. 2, pp. 181–191, 2015.

[12] F. Fresconi, G. Cooper, I. Celmins, J. DeSpirito, and M. Costello, "Flight mechanics of a novel guided spin-stabilized projectile concept," in *Proceedings of the AIAA 2010-7638, Atmospheric Flight Mechanics Conference*, 2010.

[13] R. L. McCoy, *Modern Exterior Ballistics: The Launch and Flight Dynamics of Symmetric Projectiles*, Schiffer, Atglen, PA, USA, 1999.

[14] C. H. Murphy, "Symmetric Missile Dynamic Instabilities: A Survey," in *Proceedings of the 18th AIAA Aerospace Sciences Meeting*, 1980.

[15] C. H. Murphy, "Angular motion of spinning almost symmetric missiles," *Journal of Guidance, Control, and Dynamics*, vol. 2, no. 6, pp. 504–510, 1978.

[16] C. H. Murphy, "Gravity- induced angular motion of a spinning missile," in *Proceedings of the AIAA Paper 1970-0968,<italic> Guidance, Control and Flight Mechanics Conference*, vol. 8, 1970.

[17] M. Costello and A. Peterson, "Linear theory of a dual-spin projectile in atmospheric flight," *Journal of Guidance, Control, and Dynamics*, vol. 23, no. 5, pp. 789–797, 2000.

[18] P. Wernert, "Stability analysis for canard guided dual-spin stabilized projectiles," in *Proceedings of the AIAA Atmospheric Flight Mechanics Conference*, vol. 5843, 2009.

[19] P. Wernert, F. Leopold, L. Lehmann et al., "Wind tunnel tests and open-loop trajectory simulations for a 155 mm canards guided spin stabilized projectile," in *Proceedings of the AIAA Paper 2008-6881,Atmospheric Flight Mechanics Conference and Exhibit*, 2008.

[20] G. Cooper, F. Fresconi, and M. Costello, "Flight stability of an asymmetric projectile with activating canards," *Journal of Spacecraft and Rockets*, vol. 49, no. 1, pp. 130–135, 2012.

[21] C. H. Murphy, "Instability of controlled projectiles in ascending or descending flight," *Journal of Guidance, Control, and Dynamics*, vol. 4, no. 1, pp. 66–69, 1981.

[22] D. Zhu, S. Tang, J. Guo, and R. Chen, "Flight stability of a dual-spin projectile with canards," in *Proceedings of the Institution of Mechanical Engineers Part G Journal of Aerospace Engineering*, vol. 229, pp. 704–716, 2015.

[23] K. Lloyd and D. Brown, "Instability of spinning projectiles during terminal guidance," *Journal of Guidance, Control, and Dynamics*, vol. 2, no. 1, pp. 65–70, 1979.

[24] L. C. Hainz and M. Costello, "Modified projectile linear theory for rapid trajectory prediction," *Journal of Guidance, Control, and Dynamics*, vol. 28, no. 5, pp. 1006–1014, 2005.

[25] Z. L. Liu, Y. S. Wang, and Q. Weng, "The influence of muzzle velocity on the projectile flight stability," *Journal of Projectiles, Rockets, Missiles and Guidance*, vol. 35, no. 6, pp. 48–52, 2015.